Benajes, J.; García Martínez, A.; Monsalve-Serrano, J.; Lago-Sari, R. (2018). Fuel consumption and engine-out emissions estimations of a light-duty engine running in dual-mode RCCI/CDC with different fuels and driving cycles. Energy. 157:19-30. https://doi.org/10.1016/j.energy.2018.05.144

Fuel consumption and engine-out emissions estimations of a light-duty engine running in dual-mode RCCI/CDC with different fuels and driving cycles

Jesús Benajes, Antonio García, Javier Monsalve-Serrano* and Rafael Lago Sari

CMT - Motores Térmicos, Universitat Politècnica de València, Camino de Vera s/n, 46022 Valencia, Spain

Energy
Volume 157, 15 August 2018, Pages 19-30
https://doi.org/10.1016/j.energy.2018.05.144

Corresponding author (*):
Dr. Javier Monsalve-Serrano (jamonse1@mot.upv.es)
Phone: +34 963879659
Fax: +34 963877659

Abstract

This work compares the performance and emissions of two dual-mode combustion concepts over different driving cycles by means of vehicle systems simulations. The dual-mode concept relies on switching between the dual-fuel concept known as reactivity controlled compression ignition (RCCI) and conventional diesel combustion (CDC) to cover the whole engine map. The experimental RCCI maps obtained with diesel-E85 and diesel-gasoline used as inputs to perform the simulations were obtained in a high compression ratio light-duty diesel engine (17.1:1) following the same mapping procedure in both cases. The driving cycles simulated to perform the comparison were the Real Driving Emissions cycle (Europe), Worldwide harmonized Light vehicles Test Cycle (Europe), Federal Test Procedure FTP-75 (United States) and JC08 (Japan). The results show that the dual-mode concept has potential to be implemented in flexible-fuel vehicles. Using gasoline as low reactivity fuel (LRF) for RCCI, the vehicle mileage would be equal to CDC, but having reductions in NOx and soot emissions of 16% and 50%, respectively, along the RDE cycle. Using E85 instead of gasoline, the reductions in NOx and soot emissions increase up to 50% and 85%, respectively, but in this case promoting higher thermal efficiency than CDC.

Keywords

Reactivity controlled compression ignition; Dual-mode concept; Dual-fuel combustion; Efficiency; Driving cycles

1. Introduction

In parallel to improving the aftertreatment systems to face future emissions regulations [1], the engine manufactures and the scientific community are working on developing new combustion modes to reduce the emissions generation during the combustion process [2]. This method will allow reducing the aftertreatment necessities and therefore the investment and operational costs in which this devices incur [3]. In this sense, the most expensive aftertreatment system for current compression ignition (CI) diesel engines is the selective catalytic reduction (SCR) used for NOx emissions, followed by the diesel particulate filter (DPF) for soot emissions and the diesel

oxidation catalyst (DOC) to reduce hydrocarbons (HC) and carbon monoxide (CO) emissions [3].

In the field of the new combustion modes, it has been demonstrated that the premixed low temperature combustion (LTC) concepts [4] are able to break the NOx-soot trade-off occurring with conventional diesel combustion (CDC) [5], and provide a high thermal efficiency simultaneously [6]. The most widely studied premixed LTC single-fuel concepts are the homogeneous charge compression ignition (HCCI) [7], partially premixed combustion (PPC) [8] and spark-assisted PPC [9][10]. These strategies work under highly diluted in-cylinder environments to increase the fuel-air mixing time prior to the start of the combustion and reduce the NOx and soot emissions [11]. Moreover, in these concepts, the thermal efficiency is improved due to the fast combustion processes and reduced heat transfer [12].

Nowadays, the most promising LTC concept in terms of efficiency, emissions and engine load operating range capabilities is the dual-fuel concept so-called reactivity controlled compression ignition (RCCI). Inagaki et al. [13] firstly presented this concept under the name dual-fuel premixed compression ignition (PCI) combustion. The authors reported extremely low NOx and soot emissions together with an excellent control of the combustion onset, which was possible by modifying the fuels percentages using two injector systems. Following these findings, Kokjohn et al. [14] continued developing this concept and renamed it as RCCI [15].

The RCCI concept relies on using two fuels with different reactivity injected by separated injection systems. The high reactivity fuel (HRF) is directly injected into the cylinder, while the low reactivity fuel (LRF) is injected through the intake port. Referring to the literature, it can be said that the most used HRF and LRF are diesel and gasoline, respectively [16][17]. However, RCCI can be successfully implemented using a wide variety of fuels such as ethanol [18], methanol [19], and some others [20][21][22]. As shown in previous studies, to achieve a highly efficient RCCI operation with low emissions, the major part of the total injected fuel should be LRF, while the HRF is used to trigger the combustion process [23][24]. Moreover, the HRF has a key role on the in-cylinder reactivity stratification, so that the HRF injection settings are one of the most important parameters for the combustion process development [25]. This reactivity gradient allows a more sequential autoignition than other LTC concepts [26], which reduces the pressure gradients and enables extending the operating range [27].

The potential of the RCCI concept has been recently demonstrated in different engine platforms: single-cylinder [28], multi-cylinder [29], heavy-duty [30], medium-duty [31] and light-duty diesel engines [32] operating with low [33], medium [34] and high [35] compression ratios (CR). These works conclude that, under stationary conditions, RCCI is able to achieve NOx levels below the limits proposed by the emissions regulations, together with ultra-low soot emissions [36]. Nonetheless, RCCI still has several challenges to face, such as excessive unburned HC and CO emissions during the low engine load operation [37] and too high maximum pressure rise rates (MPRR) and in-cylinder maximum pressure peaks (P_{max}) at high loads. These two limitations restrict the RCCI operating range to moderate loads, compromising its application under real engine conditions.

The dual-mode concept emerges as strategy to complete the engine map region in which the RCCI operation becomes critical either for excessive HC and CO emissions (low load) or MPRR and P_{max} (high load) [38]. This is done by switching to another combustion mode, typically CDC if a high CR is used [39]. From the technological standpoint, the modifications needed on the engine architecture to implement the dual-mode RCCI/CDC can be only justified if the aftertreatment necessities are reduced and the fuel economy is improved versus single CDC. To achieve this, the operating range covered by RCCI in the global engine map should be maximized [40].

The objective of this work is to evaluate the potential benefits of the dual-mode RCCI/CDC concept versus single CDC depending on the RCCI combustion regime coverage. The main difference of the two dual-mode concepts compared in this study is the fuels combination used to obtain the RCCI portion of the map, diesel-gasoline and diesel-E85, respectively. The experimental fuel consumption and emissions maps obtained in a high CR light-duty diesel engine (17.1:1) for both dual-mode concepts are used to obtain estimations in transient conditions through vehicle systems simulations. Transient conditions selected for the study are different driving cycles included in the homologation procedures currently in force around the world: Real Driving Emissions cycle (Europe), Worldwide harmonized Light vehicles Test Cycle (Europe), Federal Test Procedure FTP-75 (United States) and JC08 (Japan). Moreover, two additional driving cycles, New European Driving Cycle (Europe) and Artemis cycle (Europe), have been considered in the work.

2. Materials and methods

2.1. Test cell, fuels and engine description

The experimental data used as input to perform the drive cycle simulations analyzed in this work were obtained in a single-cylinder diesel engine (SCE) based on a serial production light-duty 1.9 L platform. The engine has four valves driven by dual overhead cams. The piston used is the serial one, with a re-entrant bowl that confers a geometric compression ratio of 17.1:1. The swirl ratio was fixed at 1.4 using the tangential and helical valves located in the intake port [41], which is a representative value of that used in the stock engine configuration. The Table 1 summarizes the more relevant characteristics of the engine.

Table 1. Engine characteristics.

Engine Type	4 stroke, 4 valves, direct injection
Number of cylinders [-]	1
Displaced volume [cm^3]	477
Stroke [mm]	90.4
Bore [mm]	82
Piston bowl geometry [-]	Re-entrant
Compression ratio [-]	17.1:1
Rated power [kW]	27.5 @ 4000 rpm
Rated torque [Nm]	80 @ 2000-2750 rpm

The fuel injection system was adapted to allow RCCI operation as shown in Figure 1. As sketched, the EN590 diesel fuel was injected into the cylinder by means of a centrally located solenoid direct injector (DI) coupled with a common-rail fuel injection system.

The injection settings were managed using a DRIVVEN controller. The low reactivity fuel (gasoline or E85) was fumigated in the intake manifold using a port fuel injection (PFI) located 160 mm far from the intake valves, which was governed through a Genotec unit. The mass flow rate of both fuels was measured using dedicated AVL 733S fuel balances. The main characteristics of the DI and PFI are depicted in Table 2, and the most relevant properties of the high and low reactivity fuels used in this study are summarized in Table 3.

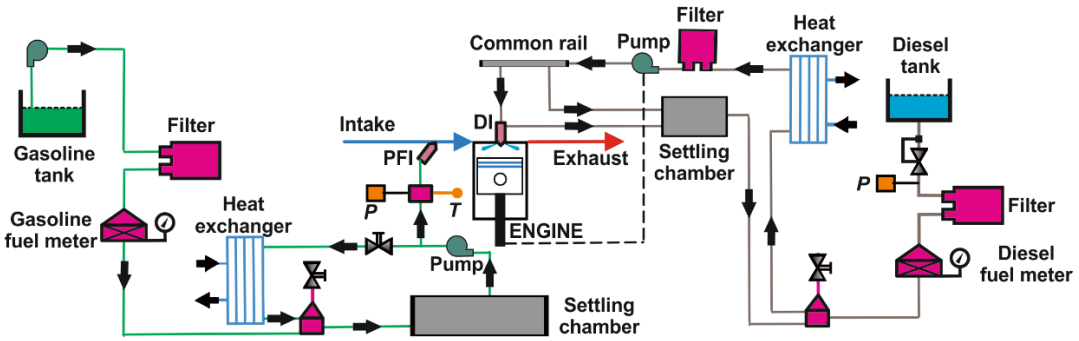

Figure 1. Fuel injection systems scheme.

Table 2. Characteristics of the direct and port fuel injector.

Direct injector		Port fuel injector	
Actuation Type [-]	Solenoid	Injector Style [-]	Saturated
Steady flow rate @ 100 bar [cm^3/min]	880	Steady flow rate @ 3 bar [cm^3/min]	980
Included spray angle [°]	148	Included Spray Angle [°]	30
Number of holes [-]	7	Injection Strategy [-]	single
Hole diameter [µm]	141	Start of Injection [CAD ATDC]	340
Maximum injection pressure [bar]	1600	Maximum injection pressure [bar]	5.5

Table 3. Physical and chemical properties of the fuels.

	Diesel EN590	Gasoline	E85
Density [kg/m^3] (T= 15 °C)	842	747	781
Viscosity [mm^2/s] (T= 40 °C)	2.929	0.545	-
RON [-]	-	97.6	108
MON [-]	-	89.7	89
Ethanol content [% vol.]	-	-	84.7
Cetane number [-]	51	-	-
Lower heating value [MJ/kg]	42.50	44.09	31.56

The scheme of test cell in which the engine is operated is shown in Figure 2. An electric dynamometer is used for the engine speed and load control during the experiments. The air intake line is composed of a screw compressor that feeds the engine with fresh air at a pressure up to 3 bar, heat exchanger and air dryer to modify the temperature and relative humidity of the air, airflow meter and a settling chamber sized to attenuate the pulsating flow. Moreover, pressure and temperature transducers are instrumented in this element with regulation purposes. The exhaust gas recirculation (EGR) is introduced in the intake line, downwards the settling chamber, through a

dedicated line composed of a heat exchanger, settling chamber and regulation valve. EGR temperature is monitored in several points along the line for its control. Finally, the pressure and temperature of the air-EGR mixture is measured in the intake manifold before entering to the cylinder.

The first elements of the exhaust line are the pressure and temperature transducers located in the exhaust manifold. After them, a settling chamber is installed to attenuate the exhaust flow before the EGR bypass. Later a pneumatic valve is used to reproduce the backpressure provoked by the turbocharger in the real multi-cylinder engine. The last elements of the exhaust line are the emissions analyzers. A five-gas Horiba MEXA-7100 DEGR analyzer is used to measure the gaseous engine-out emissions. Each steady-state operating points is measured three times along a period of 60 seconds. Finally, an AVL 415S smoke meter is used to measure the smoke emissions in filter smoke number (FSN) units. Three consecutive measurements of 1 liter volume each with paper-saving mode off were took at each engine operating point. The accuracy of the main elements of the test cell is shown in Table 4.

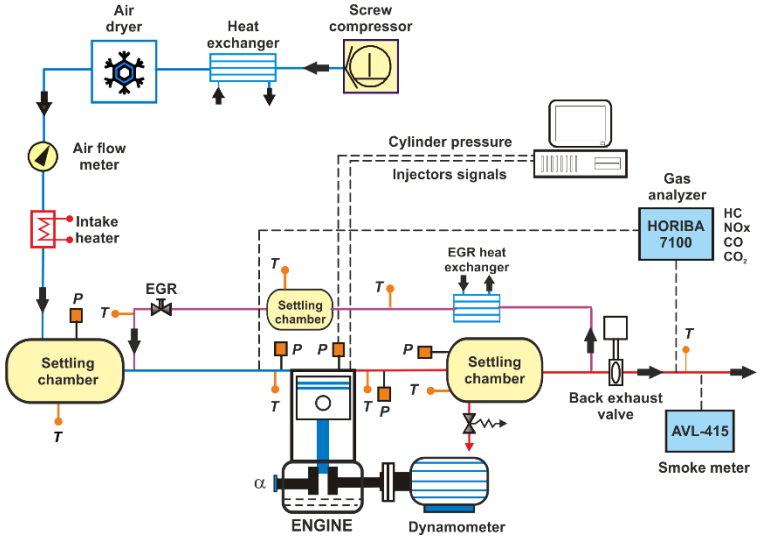

Figure 2. Test cell scheme.

Table 4. Accuracy of the instrumentation used in this work.

Variable measured	Device	Manufacturer / model	Accuracy
In-cylinder pressure	Piezoelectric transducer	Kistler / 6125BC	±1.25 bar
Intake/exhaust pressure	Piezorresistive transducers	Kistler / 4603B10	±25 mbar
Temperature in settling chambers and manifolds	Thermocouple	TC direct / type K	±2.5 °C
Crank angle, engine speed	Encoder	AVL / 364	±0.02 CAD
NOx, CO, HC, O_2, CO_2	Gas analyzer	HORIBA / MEXA 7100 DEGR	4%
FSN	Smoke meter	AVL / 415	±0.025 FSN
Gasoline/diesel fuel mass flow	Fuel balances	AVL / 733S	±0.2%
Air mass flow	Air flow meter	Elster / RVG G100	±0.1%

2.2. Dual-mode strategies description

The two dual-mode concepts studied combine CDC and RCCI combustion regimes to cover the whole engine map. The unique difference between them is the LRF used under RCCI, gasoline [38] or E85 [39]. In both cases, the HRF used is diesel EN590. Comparing both maps in Figure 3, it is seen that diesel-E85 fuel combination allows extending the RCCI operating region around 2 bar IMEP towards the high load as compared to diesel-gasoline. Moreover, with diesel-E85, the low load frontier at high engine speeds is reduced down to 1.5 bar IMEP. In RCCI combustion, the lowest operable load is restricted by the appearance of excessive HC and CO emissions, while the maximum feasible load is limited by too high MPRR. The use of E85 as LRF, instead of gasoline, allows increasing the maximum operable load due to its higher RON and MON, and enthalpy of vaporization (HoV). On the other hand, the low load RCCI region is extended with E85 because of its higher oxygen content compared to gasoline. The extra oxygen content with E85 allows using a higher diesel fraction in the low load region without exceeding the soot limitation, which contributes to reduce the HC and CO levels [39]. In both cases, the RCCI region was completed with NOx and soot emissions levels below 0.4 g/kWh and 0.01 g/kWh, respectively. In this sense, the RCCI maximum operable load was limited by the appearance of MPRR >10 bar/CAD and/or P_{max} >160 bar, while the low load frontier was limited by excessive CO levels (>5000 ppm).

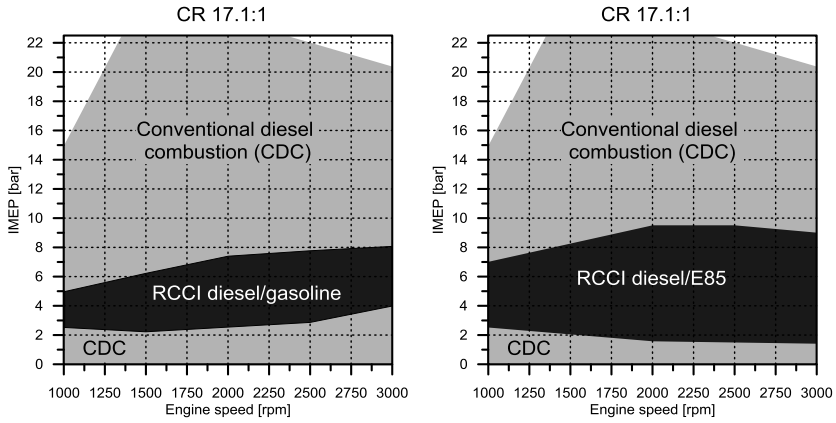

Figure 3. Illustration of the combustion strategies used to cover the engine map with the two dual-mode concepts studied: dual-mode RCCI diesel-gasoline/CDC (left) and dual-mode RCCI diesel-E85/CDC (right).

2.3. Vehicle systems and drive cycle simulations

The potential of the aforementioned dual-mode combustion strategies has been evaluated by modeling a commercial vehicle through the one-dimensional CFD software GT-Power from Gamma Technologies®. This software allows simulating predefined driving cycles, enabling to evaluate the vehicle performance on transient conditions. The performance and emissions of both dual-mode concepts were compared in several homologation cycles. Simulations were also performed for conventional diesel combustion to extend the comparison. Figure 4 shows the scheme of the dedicated model developed in GT Power. Each object represents a system part and its characteristics. The geometric and aerodynamic parameters are defined in the

vehicle object whilst the experimental engine maps for emissions and fuel consumption were set on the engine folder.

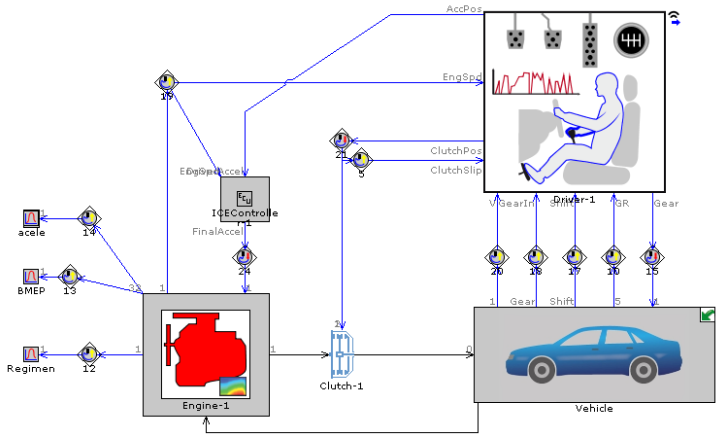

Figure 4. Simulation model built in GT-Power.

In this model, the differential equations of motion for the driveline components and the vehicle are integrated in time, calculating transient speeds and torques in the system. Engine brake mean effective pressure (BMEP) input data was calculated using indicated and friction experimental data and correlated to engine speed and accelerator position. Maps of emissions, air and fuel consumption from the engine dynamometer were used to determine emissions and fuel consumption in steady state conditions as a function of load and speed. Then, differential equations of vehicular motion were integrated in time, calculating transients of speed and torque and interpolating emissions and fuel consumption according to the load point demanded by the drive cycle condition. Rolling resistance was calculated by the model as a function of drag coefficient, rolling friction, and road grade are included in equation 1 [42], which calculates the torque required for vehicle motion.

$$\tau_{vehicle} = \left[I_{trans1} + \frac{I_{trans2}}{R_t^2} + \frac{I_{dsh}}{R_t^2} + \frac{I_{axl}}{(R_d^2)(R_t^2)} + \frac{(M_{veh})(r_{whl}^2)}{(R_d^2)(R_t^2)}\right]\frac{d\omega_{drv}}{dt} - \left[\frac{I_{trans2}}{R_t^3} + \frac{I_{dsh}}{R_t^3} + \frac{I_{axl}}{(R_d^2)(R_t^3)} + \frac{(M_{veh})(r_{whl}^2)}{(R_d^2)(R_t^3)}\right]\omega_{drv}\frac{dR_t}{dt} + \left[\frac{F_{aer} + F_{rol} + F_{grd}}{R_d R_t}\right]r_{whl} \quad (1)$$

The first term of equation represents the torque required to accelerate the effective inertia, evaluated at the clutch of the entire drivetrain. On this, I_{trans1} and I_{trans2} present the inertia in the input and output of transmission system, respectively. Likewise, I_{dsh} and I_{axl} are driveshaft and axle moment of inertia. These terms relate the number of axles and inertia of each wheel, adapted to the vehicle characteristics. R_d and R_t are terms of final drive and transmission ratio for each gear. Vehicle speed (ω_{drv}) at the instant of time (t) is directly related to the wheel radius (r_{whl}) and vehicle mass (M_{veh}). The second term of equation 1 represents the load induced by a transient gear ratio, where the vehicle object internally creates a transmission model based on the information of vehicle transmission references. External forces on vehicle are added in the third term as aerodynamic forces (F_d), rolling resistance forces (F_{rol}) and gravity forces (F_{grd}).

Table 5 specify the vehicle characteristics used in the drive cycle simulations. An Opel Vectra, which is equipped with the engine used in the bench tests, was fully described in terms of aerodynamics and mechanical characteristics. The vehicle characterization allows modeling the dragging and inertial forces that were described above.

Table 5. Vehicle specifications.

Vehicle Mass [kg]	1573
Vehicle Drag Coefficient [-]	0.28
Frontal Area [m²]	2.04
Tires Size [mm/%/inch]	225/45/R118
Vehicle Wheelbase [m]	2.7
Final Drive Ratio [-]	3.35
Gear Ratio 1st [-]	3.82
Gear Ratio 2nd [-]	2.05
Gear Ratio 3rd [-]	1.3
Gear Ratio 4th [-]	0.96
Gear Ratio 5th [-]	0.74
Gear Ratio 6th [-]	0.61

Six representative driving cycles were studied in this work: Real Driving Emissions cycle (Europe), Worldwide harmonized Light vehicles Test Cycle (Europe), Federal Test Procedure FTP-75 (United States), JC08 (Japan), New European Driving Cycle (Europe) and Artemis cycle (Europe). For the sake of clarity, the results along the paper are explained taking as reference two of the five cycles, and finally, the results of all of them are compared in summary tables (Table 8 and 9). Considering their relevance in Europe, the cycles selected to explain the results are the World Harmonized Light vehicles Test Cycle (WLTC) and a characteristic Real Driving Emissions (RDE) cycle measured by the authors [43]. The time-vehicle speed profiles for both cycles are presented in Figure 5. Comparing both cycles, it is seen that the WLTC cycle has a total duration of 1820 s (67 km) whilst the RDE presents a higher duration with a total time of 5580 s (67 km). Another difference is the total amount of accelerations and decelerations during the cycle. Since the RDE is based on real urban traffic, there is a higher number of stops and subsequently accelerations than the WLTC, which will have a direct impact on the demanded engine BMEP and engine-out emissions.

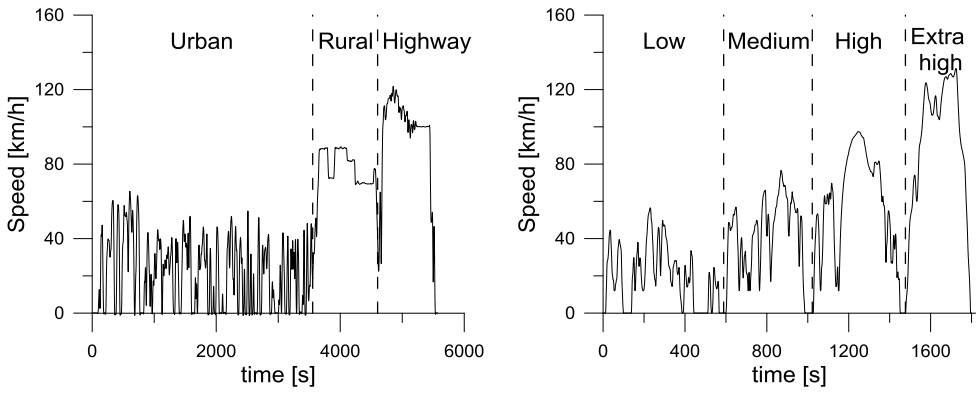

Figure 5. Time-vehicle speed profiles of the RDE (left) and WLTC (right) cycles.

Considering the maps shown in Figure 3, it is clear that the final results of the cycle will depend on the engine speed-load conditions achieved during the vehicle operation. By this reason, a preliminary study was performed to obtain the gear shifting strategy that leads to the best balance between fuel consumption and engine-out NOx and soot emissions in the WLTC cycle. As shown in Table 6, this condition is satisfied when the amount of operating points falling inside the RCCI portion of the map is maximized. Thus, the gear shifting strategy number 3 was selected for the rest of the study.

Table 6. Percentage of RCCI operating points, NOx, soot and BSFC during the WLTC for each dual-mode depending on the gear shifting strategy.

Strategy [-]	Engine speed range [rpm]	Dual-mode D-G/CDC				Dual-mode D-E85/CDC			
		RCCI points	NOx	Soot	BSFC	RCCI points	NOx	Soot	BSFC
		[%]	[g/kWh]			[%]	[g/kWh]		
1	1200-4000	22.4	2.41	0.06	319.90	47.8	2.13	0.05	349.46
2	1200-3500	26.9	1.96	0.05	308.77	61.9	1.67	0.03	340.78
3	1200-3000	33.7	1.15	0.03	284.22	70.6	0.78	0.01	319.45

3. Results and discussion

This section presents the performance and emissions simulations of both dual-mode combustion concepts. For the sake of brevity, the dual-mode concept using gasoline fuel for RCCI will be referred to as DM-G, while that using E85 for RCCI will be named as DM-E85. The first subsection is dedicated to present the maps of different parameters of both dual-mode concepts. The second one compares the emissions and performance of both dual-mode strategies and CDC over the WLTC and RDE cycles. To perform this comparison, time-cumulative results along each cycle are considered.

3.1. Dual-mode engine mapping comparison

Figure 6 shows the BSFC surface maps for both dual-mode strategies, which were obtained during the bench tests. The symbols plotted over the maps represent some operating conditions reached through the vehicle model simulation along the RDE cycle described in Figure 5 (for the sake of clarity, not all the conditions can be plotted). Different symbols are used to differentiate the three phases of the RDE cycle: urban, rural and highway. The area defined inside the white dashed lines represents the RCCI operating region in the global engine map.

From Figure 6 it can be verified that, during the RDE cycle, the majority of the operation points are below 10 bar, i.e., closer to the RCCI range. The deep blue color in the map indicates the lowest BSFC values. As it is seen, the RCCI portion of the BSFC map presents higher values with E85 than gasoline. The reasons for the BSFC increase will be discussed in the next section.

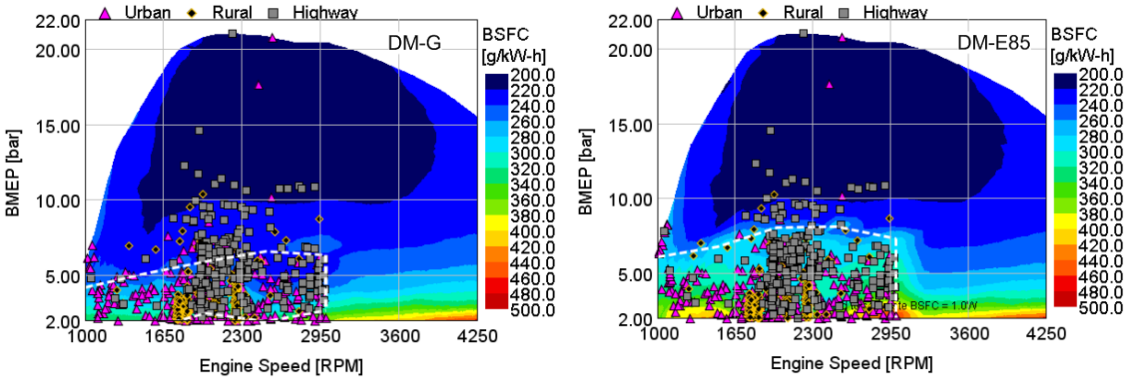

Figure 6. Operating points in brake specific fuel consumption map for DM-G concept (left) and DM-E85 concept (right) for the RDE cycle.

The lower temperatures reached during RCCI combustion combined with the smaller residence time inhibit the NOx formation, since there is not enough activation energy to initiate the Zeldovich mechanism. This fact results in a deep blue zone in Figure 7, where the maximum emission rates are near 0.6 g/kWh, notably lower than those found during CDC. Therefore, the high amount of operating conditions inside the RCCI range obtained after the gear shifting optimization is expected to allow a notable decrease in the aftertreatment demand. Finally, it is interesting to note that E85 allows extending the RCCI portion in the map, thus yielding a significant increase of the ultra-low NOx region.

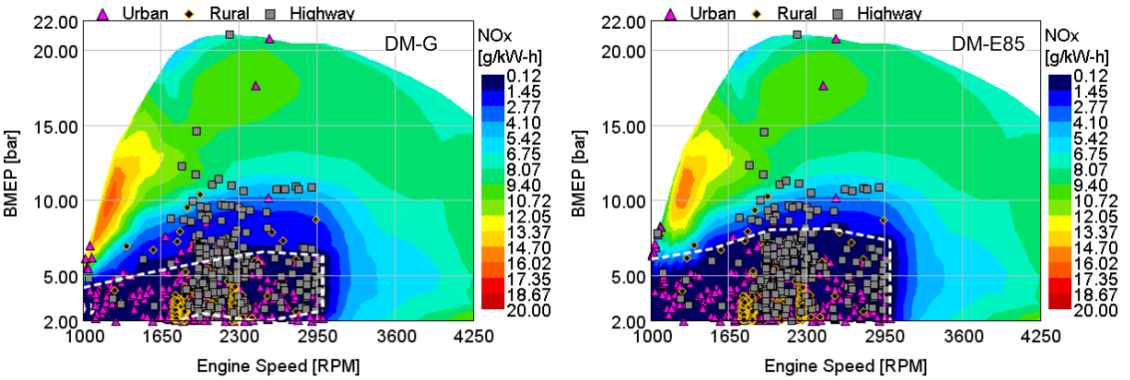

Figure 7. Operating points in NOx map for DM-G concept (left) and DM-E85 concept (right) for the RDE cycle.

Figure 8 and Figure 9 show the unburned HC and the CO emissions maps with their respective operating points. All the CDC operating range presents the diesel characteristic low emission for these two species. However, the corresponding range for RCCI has higher amounts of CO and HC due to its inherent lower combustion efficiency [37]. This is more perceptive at low engine loads conditions, where the combustion temperatures are not high enough to sustain the oxidation reactions. HC and CO levels with DM-E85 are higher than DM-G, mainly at low load, due to the higher octane number (ON) and enthalpy of vaporization (HOV) of E85, which contributes to reduce the in-cylinder temperatures.

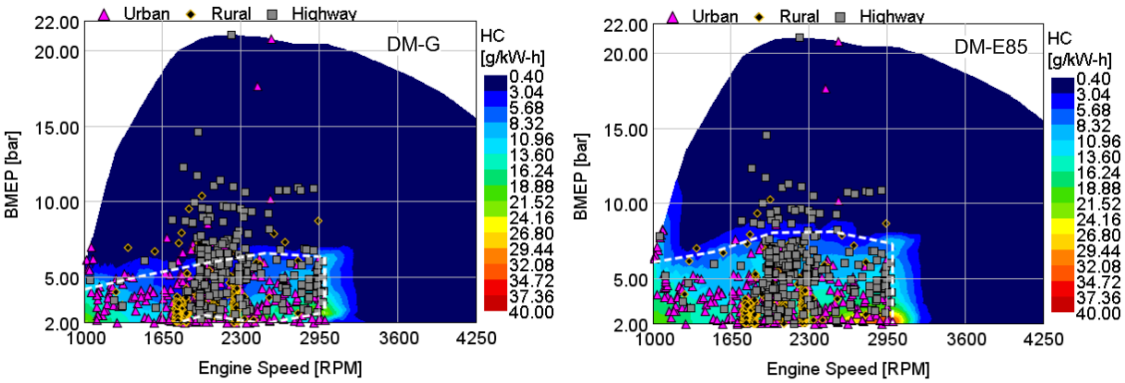

Figure 8. Operating points in unburned hydrocarbons DM-G concept (left) and DM-E85 concept (right) for the RDE cycle.

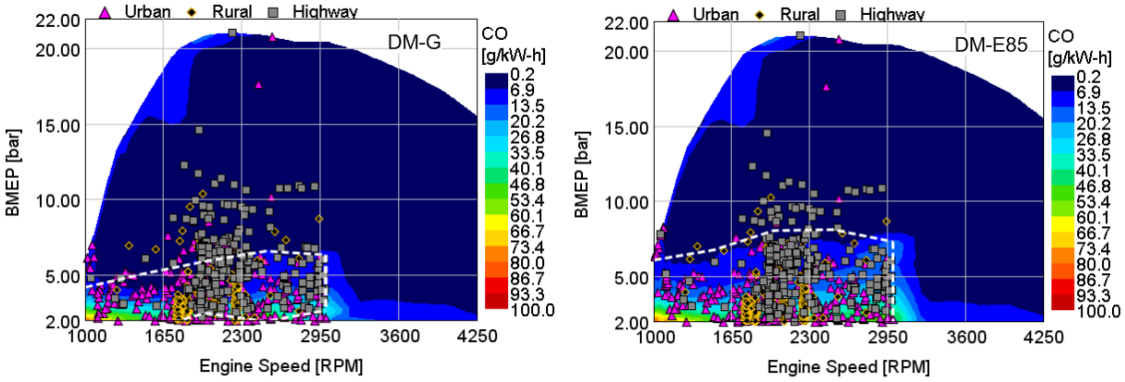

Figure 9. Operating points in CO map for DM-G concept (left) and DM-E85 concept (right) for the RDE cycle.

As shown in Figure 10, the use of RCCI combustion at low loads allows operating in almost soot-free condition. This occurs due to using a low quantity of diesel with an advanced injection timing, which results in enough mixing time to avoid the soot formation [37]. Comparing the RCCI portion of both dual-mode concepts, it is seen that DM-E85 has lower soot emissions, which is achieved, in part, due to higher oxygen content of E85 versus gasoline [21].

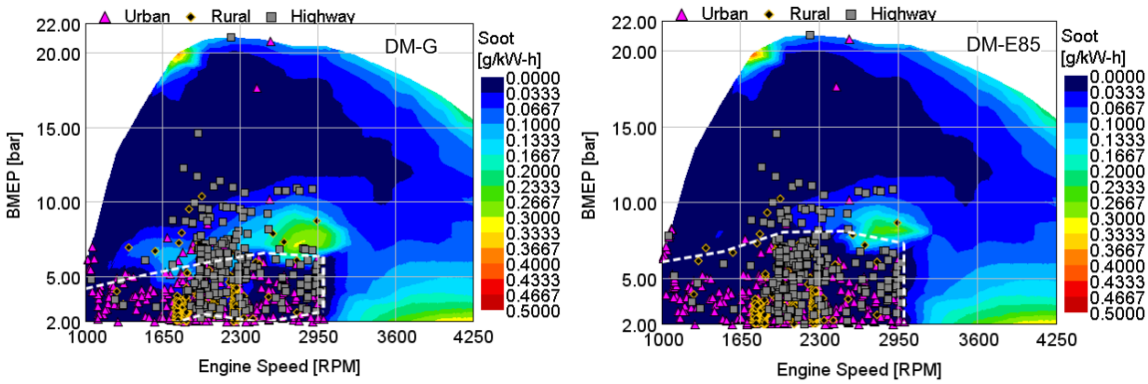

Figure 10. Operating points in brake Soot map for DM-G concept (left) and DM-E85 concept (right) for the RDE cycle.

3.2. Drive cycle fuel consumption and emissions estimation

This section presents a comparison between both dual-mode concepts and CDC in terms of the cumulative results from the WLTC and RDE drive cycles simulation. Figure 11 shows the engine load distribution along both cycles. As it can be seen, the extra high phase, for WLTC, and the highway phase, for RDE, are the phases that present a significantly portion of operating points out of RCCI conditions (BMEP >5-8 bar). For these conditions, the difference between both dual-modes are expected to be minimum. On the other hand, considering the RCCI boundaries, the differences between CDC and both dual-modes studied will be greater for the phases with the engine BMEP being lower than 5 bar.

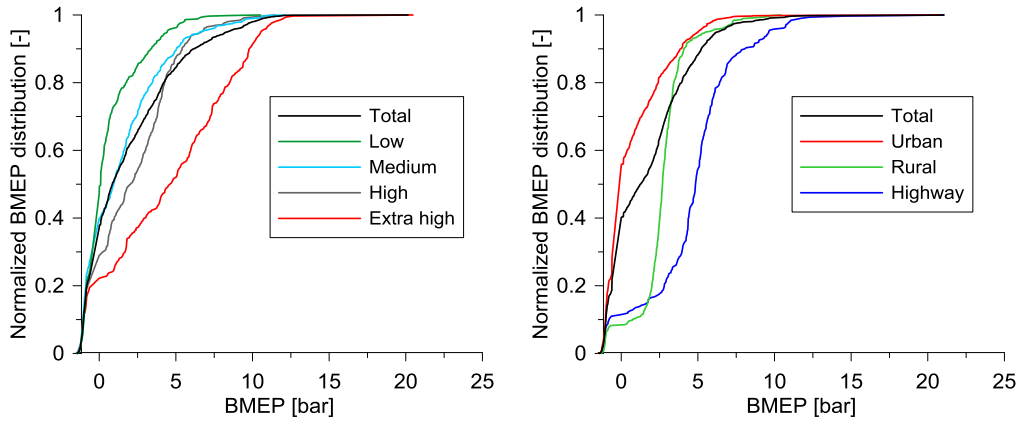

Figure 11. Cumulative frequency for the engine load in each phase of the WLTC (left) and RDE (right) cycle

Figure 12 presents the cumulative fuel consumption for each cycle and combustion mode. The text boxes included inside the graphs show the total cumulated values at the end of each phase. The fuel consumption evolution for both dual-modes has similar trend than for CDC. However, the cumulated values for both dual-modes are influenced by the BMEP distribution shown in Figure 11, which determine the quantity of operating condition that fall in the RCCI portion of the map. Comparing the trends for both cycles, it is seen that the two first phases of the WLTC and the first phase of the RDE have several conditions of idle and low power, leading to low fuel consumption. In the last phase, the vehicle reaches higher velocities and consequently higher fuel consumption. The fuel mass usage in DM-E85 is also higher for these

phases suffering an increase of almost 50% compared to the initial ones. Figure 12 also shows that the fuel consumption for CDC exceeds that of DM-G in the last phases.

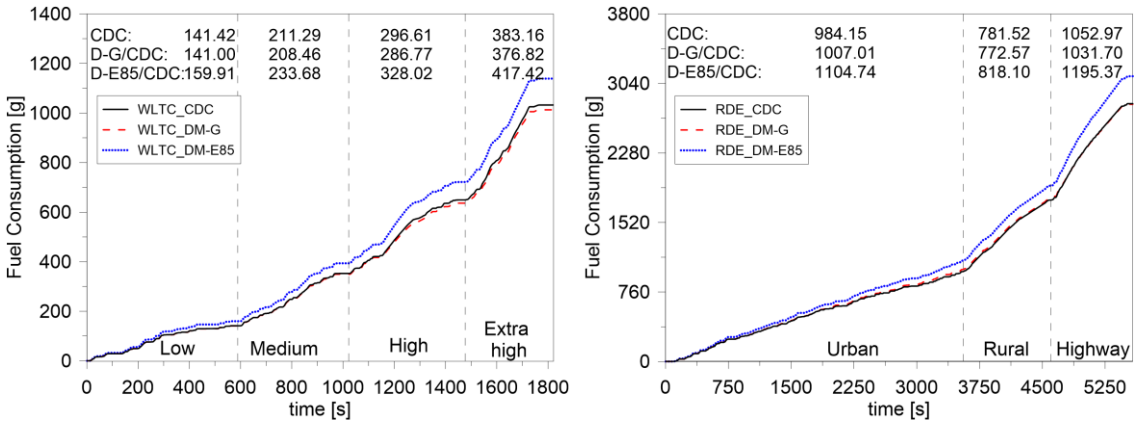

Figure 12. Cumulative fuel consumption emissions for CDC, DM-G and DM-E85 along the WLTC (left) and RDE (right) driving cycles.

Considering the lower LHV of E85 compared to the other fuels, the higher BSFC with DM-E85 cannot be directly interpreted as a lower thermal efficiency of the concept. To evaluate this fact, the combustion concepts should be compared in terms of energy. Figure 13 shows the cumulative energy consumption per cycle and combustion mode. The energy profiles have been obtained by isolating the mass consumed of each fuel, considering the LRF fraction at each operating point, and multiplying by their respective lower heating value (LHV). As it can be seen, DM-E85 presents the lowest energy consumption, which means that enables a higher fuel-to-work conversion efficiency. This behavior is confirmed in both driving cycles, confirming its higher thermal efficiency independently on the driving conditions. Analyzing the profiles, it can be inferred that the major gain with DM-E85 during the RDE cycle occurs in the rural phase, while in the case of WLTC occurs during the high phase. The benefit in these parts of the cycle compared to the DM-G is related to the greater RCCI zone in the map.

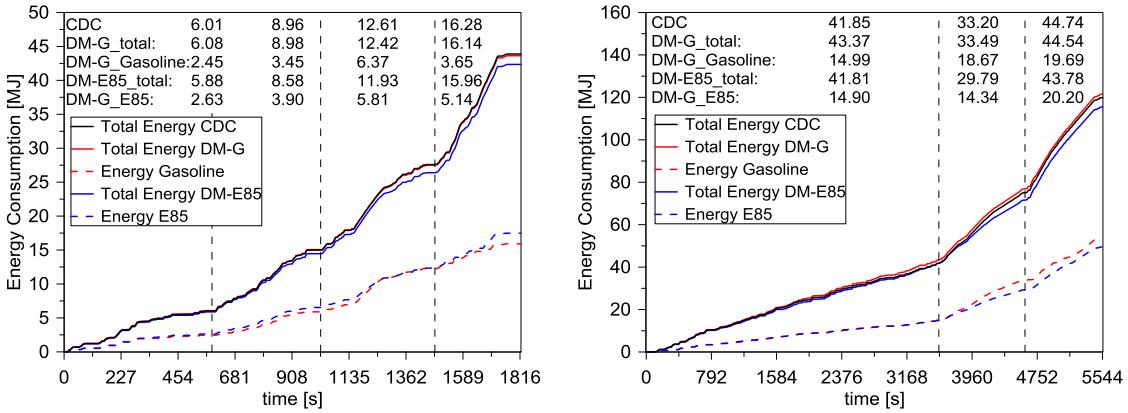

Figure 13. Cumulative energy consumption emissions for CDC, DM-G and DM-E85 along the WLTC (left) and RDE (right) driving cycles.

A key aspect for the implementation of the dual-mode concept in real vehicles is about the necessities of two fuel tanks and their sizes. From the results in Figure 12, it can be conclude that the total fuel mass needed for DM-G is almost equal than CDC. Therefore, the total volume needed for the fuel storage in both cases is expected to be

similar (similar fuel mass consumption and density). By contrast, the DM-E85 concept will require a fuel tank with higher volume to provide the same vehicle mileage. However, since the dual-mode concept has proved to be a flexible-fuel concept, it could be used the same vehicle architecture for both dual-mode concepts. In this case, sizing the fuel tank for DM-G (similar to CDC), the mileage between refueling with DM-E85 will be reduced.

A preliminary sizing of the fuel tanks can be done considering the results shown in Figure 14, in which the LRF fuel mass has been isolated considering the substitution ratio along both driving cycles. Considering the fuels properties in Table 3, the fuel volume needed for each combustion mode and drive cycle is summarized in Table 7. As it is seen, the total volume for DM-G is similar to CDC in both cycles. This means that the implementation of dual-mode concept will not incur in an additional space in the vehicle. Moreover, the diesel fuel volume needed for DM-G and DM-E85 is similar, which reinforces the thought of using a flexible-fuel vehicle architecture. The volume of the secondary fuel tank (for the LRF) needed to implement each DM with equal mileage than CDC is different. In this sense, the use of E85 requires 46% higher volume than gasoline for WLTC, and 24% more in the case of RDE, which is more representative of the real use of the vehicle.

The need of refueling for DM-E85 with a tank sized for DM-G (total volume similar to CDC) can be estimated considering the fuel tank volume of the vehicle simulated in this work (Vectra 1.9), which is 60 liters. Taking the RDE cycle as reference, the volume share needed for each fuel with DM-G concept is 54%/46% (diesel/gasoline) so that a practical fuel tank size could be 32.5/27.5 liters for the HRF and LRF, respectively. Considering the 67 km covered in the RDE cycle studied, the CDC vehicle would have a mileage of 1139 km. A DM-G vehicle would have the same mileage than CDC, while DM-E85 would have diesel for driving 1139 km and E85 for 871 km. As it is seen, the lower LHV of E85 will reduce the vehicle mileage in 268 km compared to CDC and DM-G, even having a higher thermal efficiency.

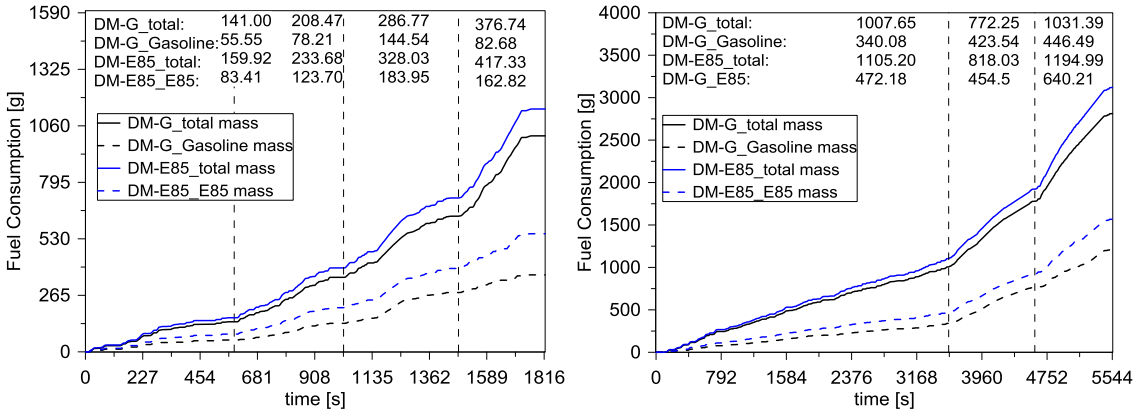

Figure 14. Cumulative fuel consumption emissions for CDC, DM-G and DM-E85 along the WLTC (left) and RDE (right) driving cycles.

Table 7. Fuel volume needed for each combustion modes and driving cycle.

Cycle	CDC	DM-G		DM-E85	
	Diesel [dm^3]	Diesel [dm^3]	Gasoline [dm^3]	Diesel [dm^3]	E85 [dm^3]
RDE	3.35	1.90	1.62	1.84	2.01
WLTC	1.23	0.77	0.48	0.69	0.71

As shown in Figure 15, both DM concepts present lower NOx emissions than CDC. The dominant mechanism for NOx formation and its respective impact on the final values of this emission was already mentioned. Therefore, the following analysis will take in to account only the effects of the driving cycles. As Figure 15 shows, the NOx emissions for all the combustion modes present an almost linear increase in both cycles up to reaching the last phase. This is a result for the high amount of low load operating conditions. Nonetheless, the cumulative values in the last phase increases in a factor of 4 for all combustion modes due to the high NOx production in the upper portion of the engine map. It is interesting to note that the cumulative NOx levels along the RDE cycle for DM-E85 are considerably lower than with CDC and DM-G, which can be attributed to the extra RCCI portion achieved with DM-E85.

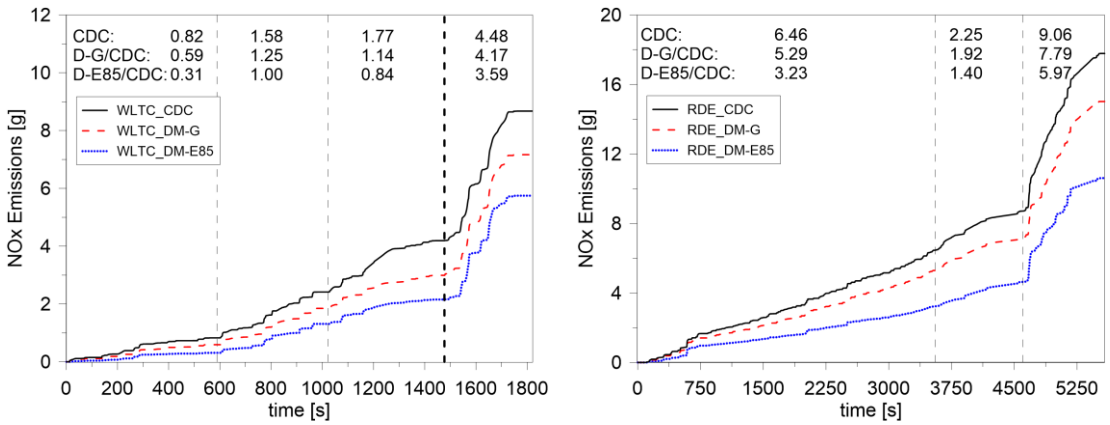

Figure 15. Cumulative NOx emissions for CDC, DM-G and DM-E85 along the WLTC (left) and RDE (right) driving cycles.

CO and HC trends shown in Figure 16 and Figure 17 are similar due to the formation mechanism of these species. Diffusive combustion presents several advantages compared to premixed mode for these pollutants. The high amount of oxygen in the flame front and the absence of premixed zone (for pure diffusive flames) allows burning efficiently all the fuel injected. By contrast, the premixed conditions founds in RCCI promote an equivalence ratio stratification, which can lead to poor burning at regions of the chamber. In addition, the in-cylinder flow can sweep part of the premixed mixture in the gaps between the piston and liner. In these zones, the combustion process cannot be supported due to the high amount of heat transfer to the walls, inhibiting the oxidation process. Therefore, the HC and CO levels increase as the RCCI range is extended. By this reason, the DM-E85 leads to substantially higher amount of these two pollutants.

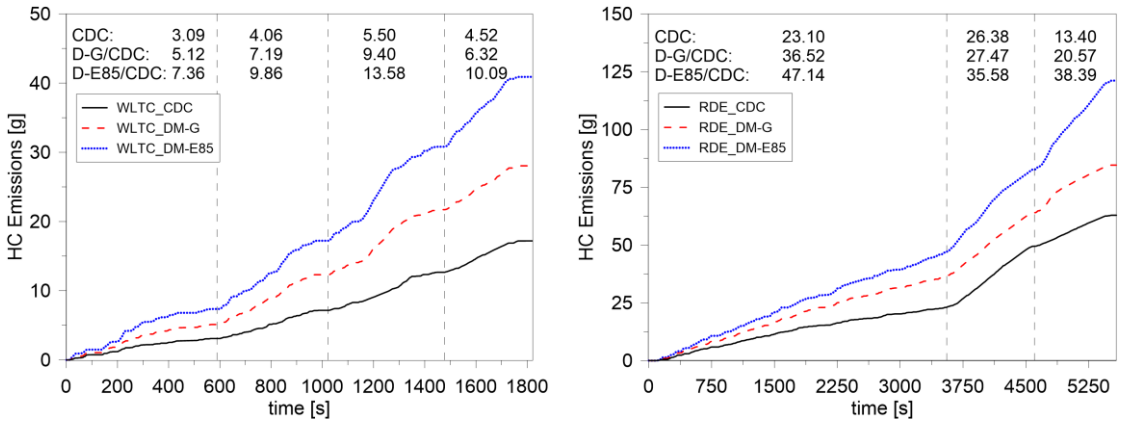

Figure 16. Cumulative HC emissions for CDC, DM-G and DM-E85 along the WLTC (left) and RDE (right) driving cycles.

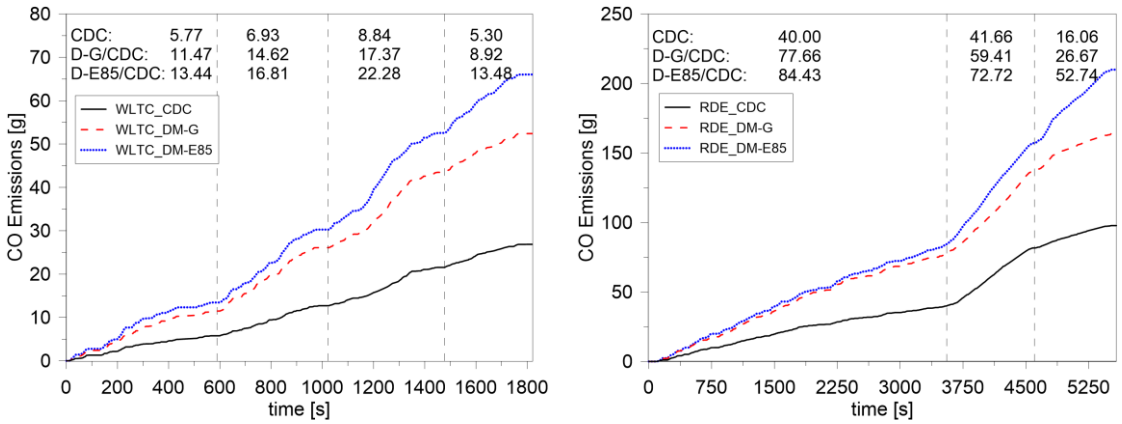

Figure 17. Cumulative CO emissions for CDC, DM-G and DM-E85 along the WLTC (left) and RDE (right) driving cycles.

The soot mechanism is related to the particle formation from the fuel molecules through their oxidation/pyrolysis process followed by its growth from process as coagulation, aggregation and surface growth [44]. The premixed flames present lower levels of soot formation because all the fuel is well mixed with air before the combustion start. Thus, the premixed phase and the higher air-fuel mixing time leads to ultra-low soot levels for RCCI. As shown in Figure 18, the use of RCCI inside the global map contributes to reduce the soot levels drastically. Due to the greater RCCI portion and the effect of soot oxidation by the oxygen from the ethanol molecule, the cumulative values for DM-E85 are very low, with only some accumulation seen in the last phases. This occurs because the majority of the operating points fall outside the RCCI area. The narrow limits of RCCI in DM-G lead to higher values of soot, but significantly lower compared to CDC levels.

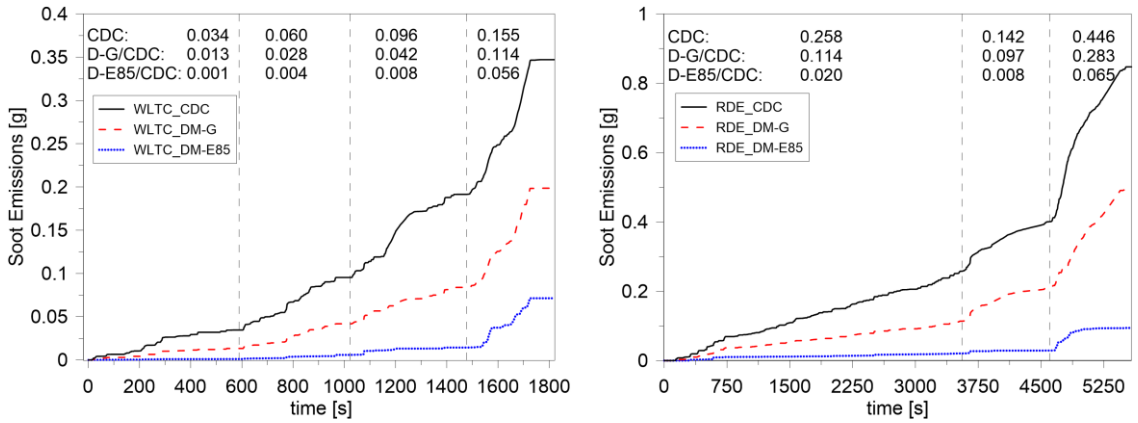

Figure 18. Cumulative Soot emissions for CDC, DM-G and DM-E85 along the WLTC (left) and RDE (right) driving cycles.

Table 8 summarizes the engine-out results for all the combustion modes and driving cycles considered in this study, whose vehicle speed-time evolutions are shown in Figure 19. The minimum values of each parameter are highlighted using an underlined bold font. From the results, it can be seen that, in spite of the differences between the drive cycles considered, there is a clear trend among the combustion modes. The DM-E85 concept presents the lowest NOx and soot emissions for all the cycles, with highest HC and CO levels. Compared to CDC, DM-E85 allows reducing NOx levels by 41 % in the RDE cycle. In the same drive cycle, the DM-G presents a reduction in this pollutant of 16 % versus CDC. Regarding HC and CO emissions, CDC results in lower emissions of these pollutants due to the diffusive combustion nature. In this sense, HC and CO emissions for DM-E85 are around 50% higher than CDC for all the cycles, while in the case of DM-G, the increase versus CDC is around 35%. Finally, both dual-mode concepts reduce the soot emissions versus CDC. Soot reduction with DM-G is around 50%, while in the case of DM-E85 the improvement is greater than 80%.

Table 8. Engine-out emissions summary for all the combustion modes and driving cycles considered in this study.

Cycle	DM-G	DM-E85	CDC	DM-G	DM-E85	CDC	DM-G	DM-E85	CDC	DM-G	DM-E85	CDC
	NOx [g/kWh]			HC [g/kWh]			CO [g/kWh]			Soot [g/kWh]		
FTP75	1.71	**1.08**	2.16	11.73	14.93	**7.23**	24.35	26.12	**12.46**	0.05	**0.01**	0.09
WLTC	2.01	**1.61**	2.43	7.87	11.47	**4.82**	14.70	18.52	**7.53**	0.06	**0.02**	0.10
Artemis	2.83	**1.52**	3.20	9.81	14.29	**6.45**	20.72	24.68	**12.01**	0.05	**0.01**	0.10
RDE	1.58	**1.12**	1.88	8.91	12.78	**6.66**	17.25	22.14	**10.35**	0.05	**0.01**	0.09
JC08	1.38	**0.84**	1.99	14.90	19.44	**8.97**	34.28	37.57	**17.34**	0.03	**0.01**	0.08
NEDC	1.21	**0.78**	1.89	11.74	15.01	**6.06**	25.79	27.81	**10.89**	0.05	**0.03**	0.11

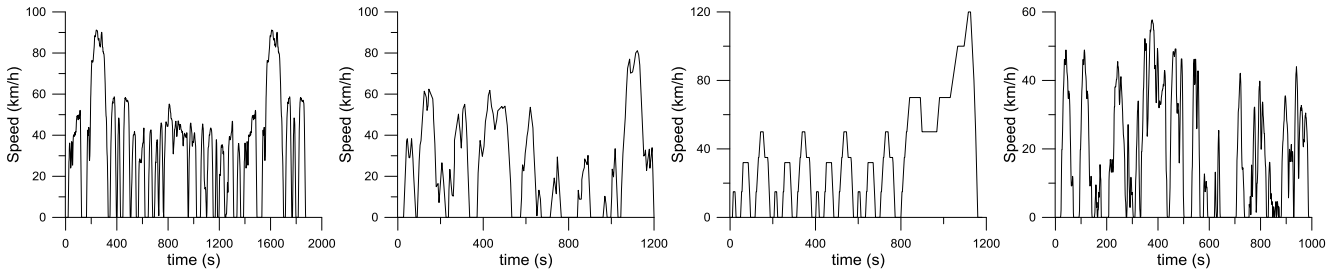

Figure 19. Time-vehicle speed profiles of the different cycles considered in this study. From the left to the right: FTP-75, JC08, NEDC and Artemis (urban).

Table 9 summarizes the specific fuel and energy consumption for all the cases. In terms of fuel mass consumption, the most efficient combustion concept whatever the drive cycle considered is the DM-G, which slightly improves the BSFC values obtained with CDC. As demonstrated in Figures 12 and 13, the fuel mass consumption with DM-E85 is penalized due to the lower LHV of E85, leading to greater BSFC than CDC. However, when considering the total energy consumption, the DM-E85 concept becomes the most efficient. This means that thermal efficiency of RCCI operating with E85 is higher than with gasoline. Finally, the table reveals that DM-G and CDC have almost the same total energy consumption.

Table 9. Specific fuel and energy consumption for all the combustion modes and driving cycles considered in this study.

Cycle	DM-G	DM-E85	CDC	DM-G	DM-E85	CDC
	BSFC [g/kWh]			Energy consumption [MJ/km]		
FTP75	**320.73**	350.46	321.46	1.90	**1.76**	1.86
WLTC	**284.22**	319.45	289.64	1.88	**1.82**	1.89
Artemis	**321.16**	364.85	325.83	2.54	**2.50**	2.53
RDE	**296.19**	328.92	298.50	1.80	**1.71**	1.78
JC08	**366.07**	409.21	367.87	1.75	**1.67**	1.74
NEDC	**304.37**	349.98	307.43	1.75	**1.74**	1.74

4. Conclusions

The present work has evaluated the potential of two dual-mode RCCI/CDC strategies by means of vehicle systems simulations. For this purpose, different driving cycles representative of the homologation procedures currently in force around the world have been compared: RDE (Europe), WLTC (Europe), FTP-75 (United States) and JC08 (Japan). Moreover, the NEDC and the Artemis cycle have been considered in the study due to their relevance in the past recent years.

In a first step, the experimental engine maps of both dual-mode concepts have been compared, highlighting which regions of the maps have the greater share to complete the RDE cycle. In this sense, the gear shifting strategy was optimized between 1200-3000 rpm to maximize operating in the RCCI portion of the map along the RDE cycle. The comparison of the maps for both combustion modes highlighted that:

- The use of E85 as LRF allows extending the RCCI operating zone, which results in a greater ultra-low NOx region, but increases the HC and CO levels in the RCCI zone. Soot levels for RCCI with E85 are lower than with gasoline.
- The BSFC in the RCCI portion of the map presents higher values with E85 than gasoline due to the lower LHV.

In a second step, the cumulative emissions and fuel consumption along the RDE and WLTC cycles were compared for both dual-mode concepts. This comparison was selected because both cycles have to be carried out complementarily during the homologation as specified in the Euro 6d-temp type-approval procedure. From these results, it was found that:

- The evolution of the accumulated emissions and fuel consumption for the WLTC and RDE have similar behavior for both combustion modes. The trends of the different phases greatly depend on the amount of operating points falling inside the RCCI operating region.
- The total fuel volume required in DM-G is almost equal than CDC. Thus, the dual-mode can be implemented without needing an additional space in the vehicle.
- A flexible-fuel architecture can be used to implement both dual-mode concepts on the same vehicle. With a fuel tank of 32.5 L for diesel and 27.5 L for the LRF, the DM-G will have the same mileage than CDC, while the mileage will be penalized in 268 km with DM-E85.

Finally, the summary of the engine-out emissions and performance results for all the driving cycles and combustion modes studied reveals that:

- DM-E85 allows reducing NOx levels by 50% in mean value over the different cycles. Considering the RDE cycle, and compared to CDC, the DM-E85 and DM-G concepts promote a 41% and 16% reduction in NOx emissions, respectively.
- HC and CO emissions for DM-E85 and DM-G are near 50% and 35% greater than CDC, respectively.
- Soot reduction versus CDC with DM-G is around 50%, while in the case of DM-E85 the improvement is greater than 80%.
- Fuel mass consumption of DM-G and CDC is almost equal, while DM-E85 fuel mass consumption becomes penalized due to the lower LHV of E85. However, the DM-E85 has the lowest energy consumption, i.e., the highest thermal efficiency.

Acknowledgments

The authors gratefully acknowledge General Motors Global Research & Development for providing the engine used to acquire the experimental data shown in this investigation. The authors also acknowledge FEDER and Spanish Ministerio de Economía y Competitividad for partially supporting this research through HiReCo project (TRA2014-58870-R).

References

[1] Fontaras G, Dilara P. The evolution of European passenger car characteristics 2000–2010 and its effects on real-world CO_2 emissions and CO_2 reduction policy. Energy Policy, Volume 49, October 2012, Pages 719-730.

[2] García-Valladolid P, Tunestal P, Monsalve-Serrano J, García A, Hyvönen J. Impact of diesel pilot distribution on the ignition process of a dual fuel medium speed marine engine. Energy Conversion and Management, Volume 149, 1 Oct 2017, Pages 192-205.

[3] Posada F.; Chambliss S.; Blumberg K. Costs of emission reduction technologies for heavy-duty diesel vehicles. ICCT White paper 2016.

[4] Zheng, M., Asad, U., Reader, G. T., Tan, Y. and Wang, M. (2009), Energy efficiency improvement strategies for a diesel engine in low-temperature combustion. Int. J. Energy Res., 33: 8–28. doi:10.1002/er.1464.

[5] Garcia A, Monsalve-Serrano J, Heuser B, Jakob M, Kremer F, Pischinger S. Influence of fuel properties on fundamental spray characteristics and soot emissions using different tailor-made fuels from biomass. Energy Conversion and Management, Volume 108, 15 January 2016, Pages 243-254.

[6] Xu G, Jia M, Li Y, Xie M, Su W. Multi-objective optimization of the combustion of a heavy-duty diesel engine with low temperature combustion under a wide load range: (I) Computational method and optimization results. Energy, Volume 126, 1 May 2017, Pages 707-719.

[7] Singh AP.; Agarwal AK. Combustion characteristics of diesel HCCI engine: an experimental investigation using external mixture formation technique. Appl Energy 2012, 99, 116–25.

[8] Manente V, Tunestal P, Johansson B et al." Effects of Ethanol and Different Type of Gasoline Fuels on Partially Premixed Combustion from Low to High Load," SAE Technical Paper 2010-01-0871, 2010.

[9] Benajes J, Molina S, García A, Monsalve-Serrano J, Durrett R. Performance and engine-out emissions evaluation of the double injection strategy applied to the gasoline partially premixed compression ignition spark assisted combustion concept. Applied Energy, Volume 134, 2014, Pages 90-101.

[10] Benajes J, Molina S, García A, Monsalve-Serrano J, Durrett R. Conceptual model description of the double injection strategy applied to the gasoline partially premixed compression ignition combustion concept with spark assistance. Applied Energy, Volume 129, 2014, Pages 1-9.

[11] Yanagihara H, Sato Y, Minuta J. "A simultaneous reduction in NOx and soot in diesel engines under a new combustion system (Uniform Bulky Combustion System e UNIBUS)," In: 17th International Vienna motor symposium; 1996.-14-303, 1996.

[12] Jin Kusaka, Takashi Okamoto, Yasuhiro Daisho, Ryouji Kihara, Takeshi Saito, Combustion and exhaust gas emission characteristics of a diesel engine dual-fueled with natural gas, JSAE Review, Volume 21, Issue 4, October 2000, Pages 489-496, ISSN 0389-4304, http://dx.doi.org/10.1016/S0389-4304(00)00071-0.

[13] Inagaki K, Fuyuto T, Nishikawa K, Nakakita K, Sakata I. Dual-Fuel PCI Combustion Controlled by In-Cylinder Stratification of Ignitability. SAE Technical Paper 2006-01-0028, 2006.

[14] Kokjohn SL, Hanson M, Splitter D, Reitz RD. Experimental Modeling of Dual-Fuel HCCI and PCCI Combustion Using In-Cylinder Fuel Blending. SAE Technical Paper 2009-01-2647, 2009.
[15] Kokjohn S L, Hanson R M, Splitter D A, Reitz R D. Fuel reactivity controlled compression ignition (RCCI): a pathway to controlled high-efficiency clean combustion, International Journal of Engine Research, 2011. Volume 12, June 2011, Pages 209-226.
[16] Li J, Yang W, Zhou D. Review on the management of RCCI engines. Renewable and Sustainable Energy Reviews, Volume 69, March 2017, Pages 65-79.
[17] Benajes J, Pastor JV, García A, Monsalve-Serrano J. An experimental investigation on the Influence of piston bowl geometry on RCCI performance and emissions in a heavy-duty engine. Energy Conversion and Management, Volume 103, October 2015, Pages 1019-1030.
[18] Sarjovaara T, Larmi M. Dual fuel diesel combustion with an E85 ethanol/gasoline blend. Fuel, 139 (2015), pp. 704–714.
[19] Zhou D, Yang W, An H, Li J, Shu C. A numerical study on RCCI engine fueled by biodiesel/methanol. Energy Conversion and Management, Volume 89, 1 January 2015, Pages 798-807.
[20] Zhang C , Zhang C, Xue L, Li Y. Combustion characteristics and operation range of a RCCI combustion engine fueled with direct injection n-heptane and pipe injection n-butanol. Energy, Volume 125, April 2017, Pages 439-448.
[21] Benajes J, Molina S, García A, Monsalve-Serrano J. Effects of low reactivity fuel characteristics and blending ratio on low load RCCI (reactivity controlled compression ignition) performance and emissions in a heavy-duty diesel engine. Energy, Volume 90, October 2015, Pages 1261–1271.
[22] Pan S, Li X, Han W, Huang Y. An experimental investigation on multi-cylinder RCCI engine fueled with 2-butanol/diesel. Energy Conversion and Management, Volume 154, 15 December 2017, Pages 92-101.
[23] Ryskamp R, Thompson G, Carder D and Nuszkowski J. The Influence of High Reactivity Fuel Properties on Reactivity Controlled Compression Ignition Combustion. SAE Technical Paper 2017-24-0080, 2017.
[24] Li Y, Jia M, Chang Y, Xie M, Reitz R. Towards a comprehensive understanding of the influence of fuel properties on the combustion characteristics of a RCCI (reactivity controlled compression ignition) engine. Energy, Volume 99, March 2016, Pages 69-82.
[25] Benajes J, Molina S, García A, Monsalve-Serrano J. Effects of Direct injection timing and Blending Ratio on RCCI combustion with different Low Reactivity Fuels. Energy Conversion and Management, Volume 99, July 2015, Pages 193-209.
[26] Najafabadi MI, Aziz NA. Homogeneous charge compression ignition combustion: challenges and proposed solutions. Journal of combustion, 2013-783, 2013.
[27] Yang Y, Dec J, Dronniou N, Sjöberg M. Tailoring HCCI heat-release rates with partial fuel stratification: Comparison of two-stage and single-stage-ignition fuels. Proceedings of the Combustion Institute, Volume 33 (2), pp. 3047-3055, 2011.
[28] Li B, Li Y, Liu H, Liu F, Wang J. Combustion and emission characteristics of diesel engine fueled with biodiesel/PODE blends. Applied Energy, Volume 206, 15 November 2017, Pages 425-431.

[29] Curran S, Hanson R, Wagner R. Reactivity controlled compression ignition combustion on a multi-cylinder light-duty diesel engine. International Journal of Engine Research 13 (3), 216-225.
[30] Benajes J, García A, Pastor JM, Monsalve-Serrano J. Effects of piston bowl geometry on Reactivity Controlled Compression Ignition heat transfer and combustion losses at different engine loads. Energy, Volume 98, March 2016, Pages 64-77.
[31] Benajes J, García A, Monsalve-Serrano J, Balloul I, Pradel G. Evaluating the reactivity controlled compression ignition operating range limits in a high-compression ratio medium-duty diesel engine fueled with biodiesel and ethanol. International Journal of Engine Research, Volume 18 (1-2), Pages 66-80, 2017.
[32] Park S, Shin D, Park J. Effect of ethanol fraction on the combustion and emission characteristics of a dimethyl ether-ethanol dual-fuel reactivity controlled compression ignition engine. Applied Energy, Volume 182, November 2016, Pages 243-252.
[33] Benajes J, Pastor JV, García A, Boronat V. A RCCI operational limits assessment in a medium duty compression ignition engine using an adapted compression ratio. Energy Conversion and Management, Volume 126, 2016, Pages 497-508.
[34] Yang B, Yao M, Cheng W, Li Y, Zheng Z, Li S. Experimental and numerical study on different dual-fuel combustion modes fuelled with gasoline and diesel. Appl Energy, 113 (2014), pp. 722–733.
[35] Li J, Yang W, Goh T, An H, Maghbouli A. Study on RCCI (reactivity controlled compression ignition) engine by means of statistical experimental design. Energy, 78, pp. 777–787, 2014.
[36] Benajes J, García A, Monsalve-Serrano J, Boronat V. An investigation on the particulate number and size distributions over the whole engine map from an optimized combustion strategy combining RCCI and dual-fuel diesel-gasoline. Energy Conversion and Management, Volume 140, 15 May 2017, Pages 98-108.
[37] Desantes JM, Benajes J, García A, Monsalve-Serrano J. The Role of the In-Cylinder Gas Temperature and Oxygen Concentration over Low Load RCCI Combustion Efficiency. Energy, Volume 78, December 2014, Pages 854–868.
[38] Benajes J, García A, Monsalve-Serrano J, Villalta D. Exploring the limits of the reactivity controlled compression ignition combustion concept in a light-duty diesel engine and the influence of the direct-injected fuel properties. Energy Conversion and Management, Volume 157, February 2018, Pages 277-287.
[39] Benajes J, García A, Monsalve-Serrano J, Villalta D. Benefits of E85 versus gasoline as low reactivity fuel for an automotive diesel engine operating in reactivity controlled compression ignition combustion mode. Energy Conversion and Management, Volume 159, March 2018, Pages 85-95.
[40] Benajes J, García A, Monsalve-Serrano J, Balloul I, Pradel G. An assessment of the dual-mode reactivity controlled compression ignition/conventional diesel combustion capabilities in a EURO VI medium-duty diesel engine fueled with an intermediate ethanol-gasoline blend and biodiesel. Energy Conversion and Management, Volume 123, July 2016, Pages 381-391.
[41] Olmeda P, Martin J, Garcia A, Villalta D, Warey A, Domenech V. A Combination of Swirl Ratio and Injection Strategy to Increase Engine Efficiency. SAE International Journal of Engines 10(3):2017, doi:10.4271/2017-01-0722.

[42] GT-Suite. Engine performance application manual, 2016.
[43] Luján JM, Bermúdez V, Dolz V, Monsalve-Serrano J. An assessment of the real-world driving gaseous emissions from a Euro 6 light-duty diesel vehicle using a portable emissions measurement system (PEMS). Atmospheric Environment, Volume 174, Feb 2018, Pages 112-121.
[44] Heywood, J. Internal Combustion Engines Fundamentals.McGraw-Hill,1988.

Abbreviations

ATDC: After Top Dead Center

CAD: Crank Angle Degree

CDC: Conventional Diesel Combustion

CI: Compression Ignition

CO: Carbon Monoxide

CR: Compression Ratio

DI: Direct Injection

DOC: Diesel Oxidation Catalysts

DPF: Diesel Particulate Filter

EGR: Exhaust Gas Recirculation

FSN: Filter Smoke Number

HC: Hydro Carbons

HCCI: Homogeneous Charge Compression Ignition

HoV: Enthalpy of Vaporization

HRF: High Reactivity Fuel

IMEP: Indicated Mean Effective Pressure

LRF: Low Reactivity Fuel

LTC: Low Temperature Combustion

MON: Motored Octane Number

MPRR: Maximum Pressure Rise Rate

NOx: Nitrogen Oxides

PCI: Premixed Compression Ignition

PFI: Port Fuel Injection

PPC: Partially Premixed Charge

RCCI: Reactivity Controlled Compression Ignition

RON: Research Octane Number

SCE: Single Cylinder Engine

SCR: Selective Catalytic Reduction